



Article

# Development of Sugarcane Bagasse Ash Blended Cementitious Composites Reinforced with Carbon Nanotubes and Polypropylene Fibers

Muhammad Ayyan Iqbal<sup>1</sup>, Umbreen Us Sahar<sup>1</sup> , Alireza Bahrami<sup>2,\*</sup> , Noor Yaseen<sup>1,3</sup> and Iffat Siddique<sup>4</sup>

<sup>1</sup> Department of Civil Engineering, University of Engineering and Technology, Lahore 54000, Pakistan

<sup>2</sup> Department of Building Engineering, Energy Systems and Sustainability Science, Faculty of Engineering and Sustainable Development, University of Gävle, 801 76 Gävle, Sweden

<sup>3</sup> Directorate General Small Dams, Irrigation Department, Khyber Pakhtunkhwa, Pakistan

<sup>4</sup> Department of Civil Engineering, University of Management and Technology, Lahore 54000, Pakistan

\* Correspondence: alireza.bahrami@hig.se

**Abstract:** Cement-based composites, as primary construction materials, have undergone significant advancements over the years, yet researchers still face challenges in terms of their durability and impact on the environment. The goal of this research is to develop environmentally friendly cementitious composites blended with sugarcane bagasse ash (SCBA) and reinforce them with multi-walled carbon nanotubes and polypropylene (PP) fibers. Because of the high cost associated with carbon nanotubes (CNTs) and PP fibers, as well as CO<sub>2</sub> emission, which affect the economic and environmental aspects of this field, an agricultural waste such as SCBA was introduced in the current study that is both economically and environmentally viable. For this purpose, five mixes were designed by varying the CNTs content whilst keeping the PP fibers and SCBA contents constant at 1.5% and 15% by weight of the binder (ordinary Portland cement + SCBA), respectively. The developed blends were tested for various mechanical and durability properties, i.e., compressive strength, flexural strength, impact strength, water absorption, and ultrasonic pulse velocity. Moreover, the microstructures of the newly developed low-carbon SCBA-based composites reinforced with PP fibers and CNTs were studied through scanning electron microscopy and energy dispersive spectroscopy. The results showed that the developed blends incorporating 15% SCBA, 1.5% PP fibers, and 0.08% CNTs, by weight of the binder, demonstrated the compressive, flexural, and impact strengths as 15.30 MPa, 0.98 MPa, and 0.11 MPa, respectively. The investigated blends proved to be cost-effective and environmentally beneficial, rendering them suitable for utilization in general construction and maintenance works.

**Keywords:** carbon nanotube; polypropylene fiber; Portland cement; sugarcane bagasse ash; blended cementitious composite



**Citation:** Iqbal, M.A.; Sahar, U.U.; Bahrami, A.; Yaseen, N.; Siddique, I. Development of Sugarcane Bagasse Ash Blended Cementitious Composites Reinforced with Carbon Nanotubes and Polypropylene Fibers. *J. Compos. Sci.* **2024**, *8*, 94. <https://doi.org/10.3390/jcs8030094>

Academic Editor: Francesco Tornabene

Received: 23 December 2023

Revised: 18 January 2024

Accepted: 23 February 2024

Published: 4 March 2024



**Copyright:** © 2024 by the authors. Licensee MDPI, Basel, Switzerland. This article is an open access article distributed under the terms and conditions of the Creative Commons Attribution (CC BY) license (<https://creativecommons.org/licenses/by/4.0/>).

## 1. Introduction

The cement industry accounts for 8% of global carbon dioxide (CO<sub>2</sub>) emissions [1–5]. During the production of cement, limestone (CaCO<sub>3</sub>) is calcined at a high temperature of 1300 °C to 1400 °C, resulting in clinkers, which mainly consist of calcium disilicate (C<sub>2</sub>S) and calcium trisilicate (C<sub>3</sub>S). The calcination of calcium carbonate (CaCO<sub>3</sub>) results in the release of CO<sub>2</sub> gas [6,7]. Also, fossil fuels are burned in large quantities to achieve the aforementioned temperature for the calcination of limestone, which results in huge emissions of CO<sub>2</sub>. The increasing concentration of CO<sub>2</sub> is one of the major contributing factors to global warming. To reduce the carbon footprint of cement as well as to compensate for the relatively high cost of cement and reinforcements, supplementary cementitious materials (SCMs) have been introduced as partial cement replacements to make cementitious composites economical, green, and sustainable [8]. The scholars have extensively studied conventional SCMs, such as fly ash, silica fume, bentonite clay, and ground granulated blast

furnace slag [9–14]. While the research on unconventional SCMs, including agricultural wastes such as sugarcane bagasse ash (SCBA) and rice husk ash, in the development of sustainable construction materials is still in its early stages [15–22].

The availability of SCMs varies demographically. SCBA is a waste product of the sugarcane industry. It is rampantly available in the subcontinent as the annual production of SCBA is approximately 10 million tons, and it is formed from the burning of sugarcane bagasse for power production [23]. The pozzolanic activity of SCBA has been widely reported in the literature. SCBA is mainly composed of silicon dioxide ( $\text{SiO}_2$ ), whereby it reacts with calcium hydroxide (C-H), a hydration product of the cement hydration, to form additional calcium silicate hydrate gel (C-S-H) [24–26]. Research works performed on the partial replacement of cement with SCBA indicated that SCBA improved the mechanical properties of cementitious composites when used in an optimum quantity (10–20% by weight of binder) [27,28]. SCBA also enhanced the resistance of cementitious composites against acid attacks and chloride due to its superior pozzolanic activity, making the resulting composites durable and sustainable [29,30]. The workability of cementitious composites is improved as well. However, a higher replacement of cement with SCBA compromised the strength and durability of cementitious composites owing to the excess leaching out of silica from the internal matrix. This discrepancy can be compensated by the addition of optimum concentrations of microfibers, like polypropylene (PP) fibers and polyvinyl alcohol (PVA) fibers [28,31,32]. Since SCBA is a waste product and is cheaper and readily available, using it as a partial replacement for cement has certainly reduced the construction capital [8,30,33].

Conventional cement-based materials are vulnerable to cracking due to their brittle nature and low tensile strength. To compensate for the brittleness and low tensile strength, microfibers and nanoparticles can be introduced into concrete to enhance the performance at the micro- and nano-levels where the cracks begin to propagate [34–36]. To improve the tensile strength, ductility, and fracture strength, microfibers including PP fibers, PVA fibers, steel fibers, glass fibers, etc., are commonly utilized in concrete, leading to the production of fiber-reinforced concrete (FRC) [37,38]. Each type of the fibers is unique in its strength, availability, and cost. Amongst all synthetic fibers, PP fibers are lightweight, resistant to corrosion, and relatively cheaper [34]. Their energy absorption capacity and crack bridging properties limit the formation of cracks owing to the dry shrinkage and impact loading, enhancing the durability, sustainability, and serviceability of concrete [39].

PP fibers improve the performance of cementitious composites at both meso- and micro-levels. The advancement in technology has introduced nanomaterials like graphene, graphene oxides, and carbon nanotubes (CNTs) in concrete-based research [40–44]. Of all nanomaterials, the main focus of the present research is the use of CNTs. CNTs are tubes of carbon atoms with nanometric diameters and can be either single-walled (SW-CNTs) or multi-walled (MW-CNTs) [45]. SW-CNTs exhibit a tensile strength of 500 GPa, and MW-CNTs present a tensile strength of 10–63 GPa. Young's modulus of SW-CNTs is about 1 TPa, and that of MW-CNTs is approximately 0.21 GPa according to the literature [46–48]. CNTs, due to their Young's modulus, crack-bridging properties, energy absorption capabilities, and densification properties, enhance the mechanical and durability properties of cementitious composites. The small size of CNTs allows them to be dispersed at a finer scale when compared with traditional reinforcing synthetic fibers [34,49,50]. The inclusion of CNTs into a cementitious system can strongly reinforce the cement–sand matrix by filling the nanopores between the C-S-H gel and C-S-H with increased high-stiffness [47,51]. Although extensive research has been carried out on the incorporation of CNTs in cementitious composites, the mechanism by which CNTs reinforce and impart their properties to cementitious composites remains incomprehensible owing to the flexibility in their dispersion, bonding, and manufacturing processes.

The hybrid effects of CNTs and PP fibers have been examined in the literature. CNTs and PP fibers enhance mechanical and durability properties when used in optimum quantities, i.e., 0.25% and 1.5% by weight of the binder, respectively, in cementitious composites [38,52]. The residual fracture energy is improved by a hybrid mix of CNTs and PP

fibers because of the mitigation of the crack formation at the nano- and micro-levels [34,53], which highlights the promising potential of this optimized combination to enhance the sustainability of cementitious composites.

A review of the existing literature revealed that studies on the co-existence of SCBA and CNTs in concrete are not well documented. Several studies have used alternate materials, like bagasse fiber, fly ash, basalt fibers, and metakaolin, in combination with CNTs in cement-based composites [54–57]. CNTs can impart mechanical properties, whereas SCBA can improve the economy, reduce the carbon footprint of cementitious composites, and enhance the strength and durability of cement-based materials [8,30,33,52,58]. Therefore, to address both the economic and environmental aspects of the construction industry, the present study is a step toward developing sustainable cement-based materials by utilizing locally available SCBA in cementitious composites with the addition of CNTs and PP fibers.

The main objective of this study is to develop SCBA-based green cementitious composites reinforced with PP fibers and MW-CNTs. The effects of the CNT variation on SCBA-blended PP-fiber-reinforced cementitious composites were explored, thereby combining the advantages of both CNTs and PP fibers for the strength and durability while reducing the most significant disadvantage of cementitious composites, namely, their carbon footprint. The PP fibers content was kept constant at 1.5% by weight of the binder, and 15% of cement was replaced by SCBA. The concentration of CNTs by weight of the binder was varied to determine their effects on SCBA-blended cementitious composites reinforced with PP fibers by conducting mechanical and durability tests. In addition, the microstructure of cementitious composites was analyzed by performing scanning electron microscopy (SEM) and energy dispersive spectroscopy (EDS).

## 2. Methodology

The methodology opted for this study involved material processing, mix design, batching of materials, stirring and sonication of CNTs, casting, curing, and finally, experimentation. The experimental methodology adopted in this research is summarized in Figure 1.

### 2.1. Materials

Ordinary Portland cement (OPC) was utilized as the main binder in the mix proportion. SCBA, after its collection from a dumped landfill, was sieved through a No. 50 (mesh size of 0.300 mm) sieve, followed by drying it in an oven at 110 °C. It is worth noting that SCBA was not subjected to any additional processing (such as grinding or burning at higher temperatures) to make its use more viable and sustainable [20]. Afterward, it was used as partial cement replacement in the mix design process, as detailed in Section 2.3. The chemical compositions of OPC and SCBA were determined employing the X-ray fluorescence analysis, and the results are listed in Table 1.

**Table 1.** Chemical composition of OPC and SCBA (%).

	CaO	MgO	SiO <sub>2</sub>	SO <sub>3</sub>	Al <sub>2</sub> O <sub>3</sub>	Fe <sub>2</sub> O <sub>3</sub>	LOI
OPC	62.32	2.75	20.53	2.47	5.10	2.96	1.58
SCBA	2.24	1.80	69.80	0.46	1.15	1.95	19.30

Natural river sand was utilized as fine aggregate. The specific gravity and water absorption of sand, as determined following ASTM C128 [59], were found to be 2.69 and 1.07%, respectively. The particle size distribution of fine aggregate is displayed in Figure 2. It can be seen that the particle gradation for sand was within the limits specified by ASTM C33 [60].

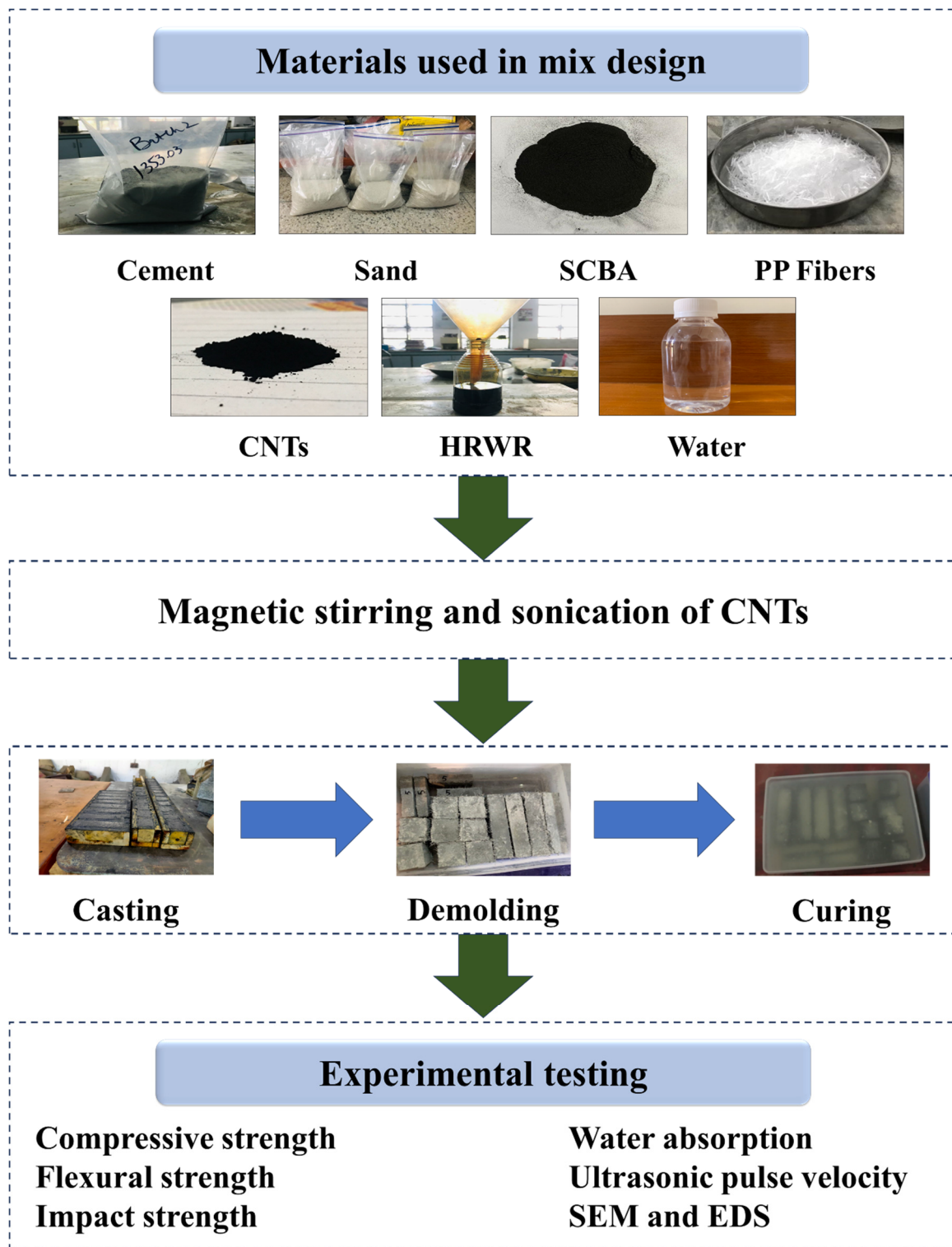
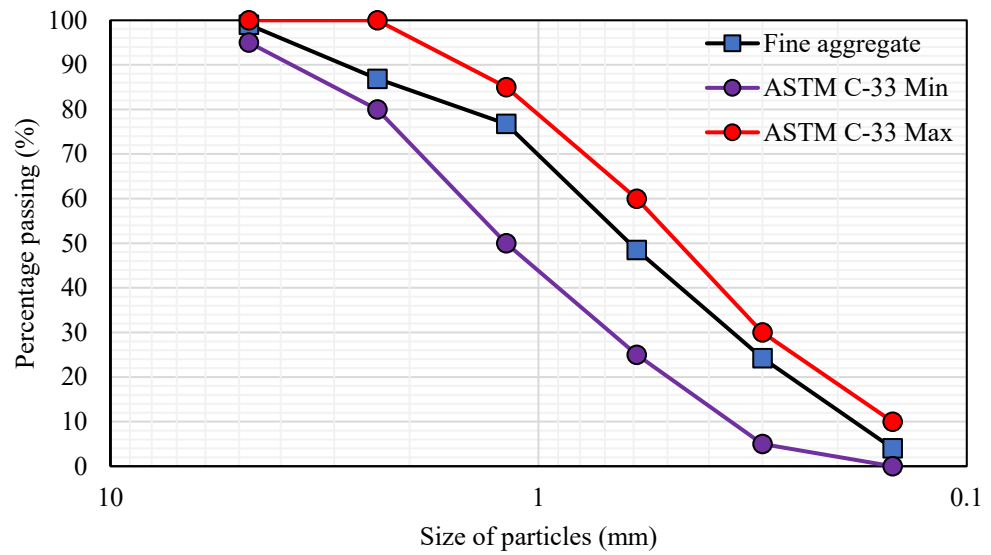


Figure 1. Experimental overview of current study.

PP fibers with a diameter of 0.5 mm, aspect ratio of 38, tensile strength of 5250 psi, and specific gravity of 0.9 were used. CNTs with outer diameters ranging from 20 to 40 nm, a density of 0.07 g/cm<sup>3</sup>, and purity of >90% were utilized in the current research. Chemrite-NN, a poly-naphthalene-based high-range water reducer (HRWR) or superplasticizer, was used to improve the workability of the mortar mix and serve as a surfactant for the dispersion of CNTs within the cementitious matrix.



**Figure 2.** Particle size distribution of fine aggregate.

2.2. Magnetic Stirring and Sonication of CNTs

Dispersion of CNTs in a liquid called a surfactant is a prerequisite to enable their use in a cementitious system. If not properly dispersed, due to strong Van Der Waals force, CNTs will agglomerate, and they will not be able to distribute uniformly in the cement–sand matrix [61–65].

For the dispersion of CNTs, a naphthalene-based superplasticizer was utilized as a surfactant [66]. The apparatus used for dispersion is depicted in Figure 3. The method of magnetic stirring followed by bath sonication was adopted. CNTs were mixed in the surfactant employing a hot plate magnetic stirrer to prepare the solution for the sonication process. The ratio of CNTs to surfactant was kept at 1:4 in accordance with the literature [51,66]. The solution was diluted using 100 mL of distilled water. Magnetic stirring was then carried out at a medium speed while covering the beaker with aluminum foil for 30 min. After magnetic stirring was conducted, the solution was transferred to a bath sonicator, which utilized the infrared radiation to disperse CNTs into the solution. The process was continued for an hour, and the temperature of the water bath was maintained at  $28 \pm 2 \text{ }^\circ\text{C}$  using ice cubes.



**Figure 3.** Apparatus used for sonication of CNTs: (a) Magnetic stirrer, (b) Bath sonicator.

2.3. Mix Design

The mix design of this research inhibited two different types of binders, namely OPC and SCBA, and two different types of reinforcements, namely PP fibers (micro reinforcement) and MW-CNTs (nano reinforcement). Five different mixes were developed. The

first mix comprised of 100% OPC without additives, and it was termed as the control (represented as C). The second mix (designated as M1) comprised of 15% SCBA as a partial replacement of OPC. The third mix (denoted as M2) comprised of 15% SCBA with an optimum percent dosage of PP fibers as 1.5% by weight of the binder (OPC + SCBA) as per the literature [38,67]. The fourth and fifth mixes (M3 and M4) incorporated corresponding percent dosages of CNTs of 0.04% and 0.08% by weight of the binder, wherein the contents of SCBA and percent dosage of PP fibers in both mixes were 15% and 1.5% by weight of the binder, respectively. The concentration of HRWR was kept constant at 8% by weight of the binder. The details of the mix proportions are presented in Table 2. As an example, C100-S0-P0-CN0 indicates 100% OPC, 0% SCBA, 0% PP fibers, and 0% CNTs, which is the control mix as C.

**Table 2.** Mix proportions of developed composites (kg/m<sup>3</sup>).

Mixes	Short Descriptions of Mixes	OPC	SCBA	Sand	Water	CNTs	PP Fibers	HRWR
C	C100-S0-P0-CN0	666.67	0	1833.3	323.3	0	0	53.3
M1	C85-S15-P0-CN0	566.67	100	1833.3	323.3	0	0	53.3
M2	C85-S15-P1.5-CN0	566.67	100	1833.3	323.3	0	10	53.3
M3	C85-S15-P1.5-CN0.04	566.67	100	1833.3	323.3	0.27	10	53.3
M4	C85-S15-P1.5-CN0.08	566.67	100	1833.3	323.3	0.53	10	53.3

A Hobart-Model A200 mixer was employed to mix the materials. The mixing was completed in four stages at  $16 \pm 2$  °C, over the course of ten minutes, as illustrated in Figure 4. The mixer was paused at 1.5, 4, and 5.5 min to remove the adhering materials from the sides and bottom of the bowl. The mortar mixtures were poured into wooden molds, and they were de-molded after 24 hours, followed by 28 days of water curing.

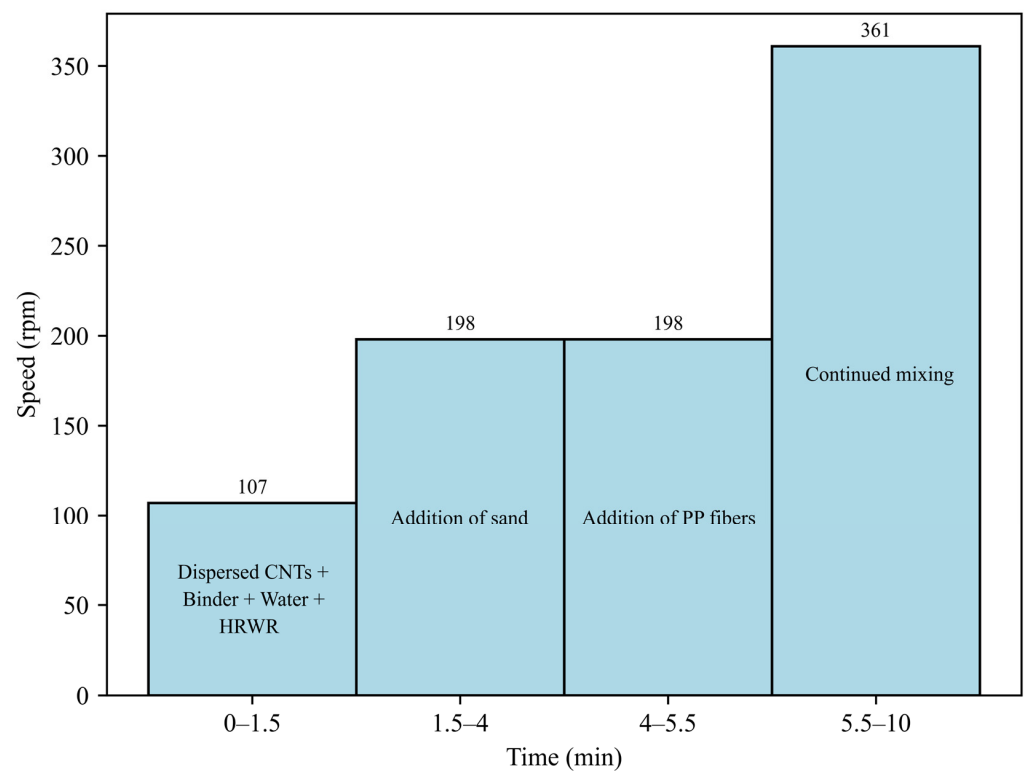


**Figure 4.** Pictorial form of mixing procedure (horizontal axis is not on scale).

#### 2.4. Test Methods

The test setups for different test methods followed in this research work are shown in Figure 5. For the compressive strength tests, a 100-ton universal compression testing machine was used, and four cubes (50 mm × 50 mm × 50 mm) were casted for each mix in accordance with ASTM C109 [68]. Three-point flexural strength test was performed on four samples (40 mm × 40 mm × 160 mm) utilizing the Shimadzu universal testing machine according to ASTM C348-20 [69]. The impact strength test was conducted on four samples employing the Charpy impact test machine (25 mm × 25 mm × 100 mm) in accordance with ASTM E23 [70].

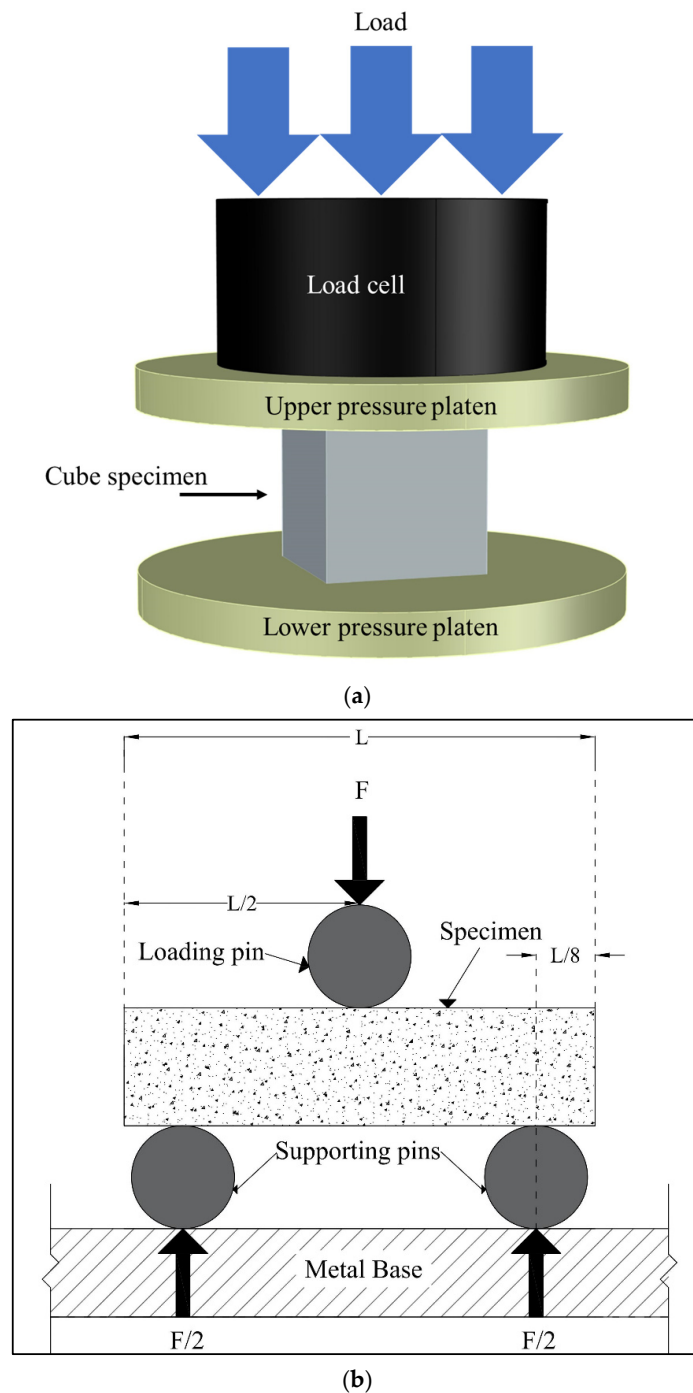
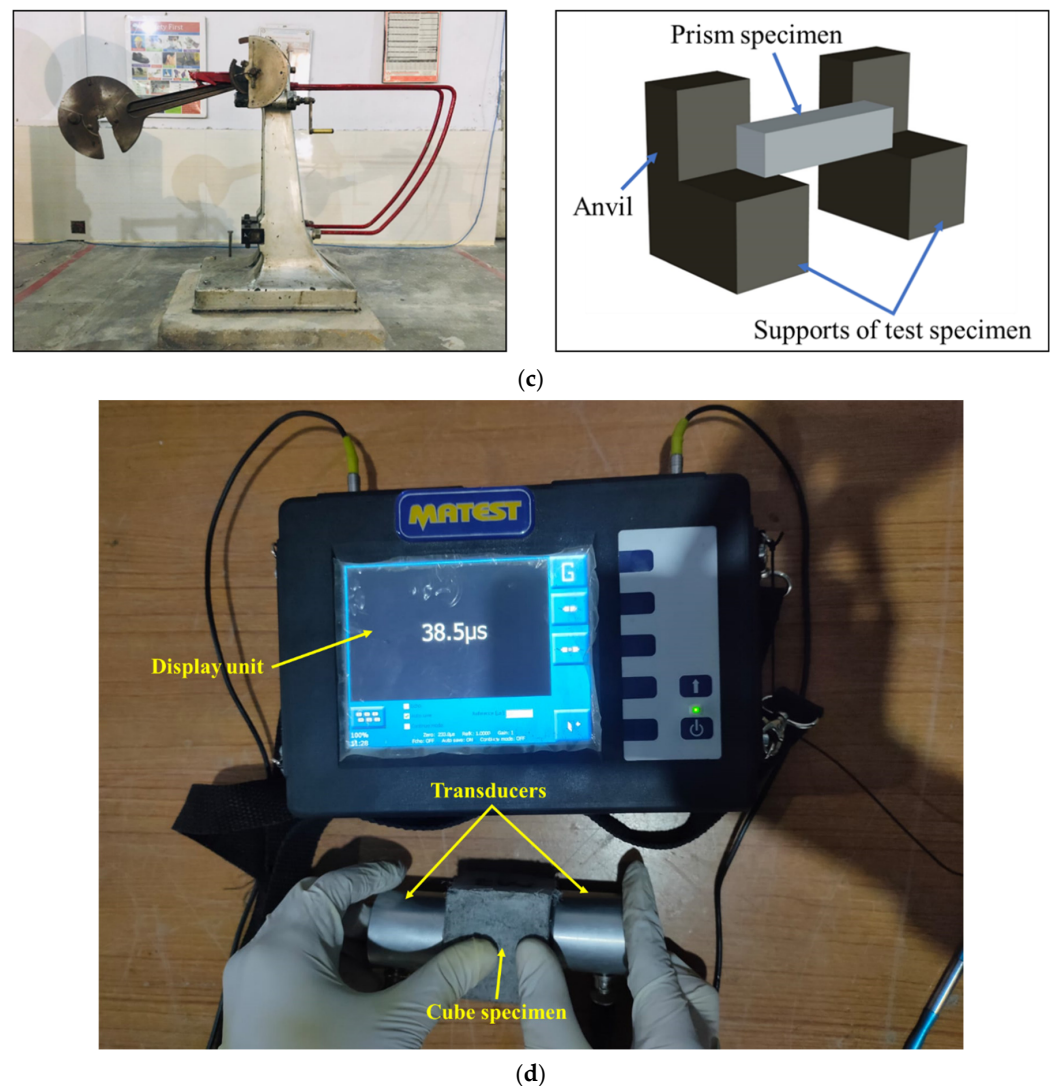


Figure 5. Cont.



**Figure 5.** Appearances of different test assemblies: (a) Compressive strength test, (b) Flexural strength test (source of image: Yaseen et al. [20]), (c) Impact strength test, (d) Ultrasonic pulse velocity (UPV) test.

For each mix, three cubes (50 mm × 50 mm × 50 mm) were tested for the water absorption and UPV based on ASTM C1403-00 [71] and ASTM C597-16 [72], respectively. For the microstructural analysis of the developed mixes, the specimens were examined through SEM and EDS after testing for their mechanical properties.

### 3. Results and Discussion

#### 3.1. Compressive Strength Test

The results of the compressive strength test are displayed in Figure 6. According to the test results, the control mix (C) demonstrated a compressive strength that was 9.3% higher than mix M1. This is consistent with the result of a previous study [27]. The decrease in the compressive strength could be attributed to the OPC dilution effect, in which case the larger SCBA particles replace a significant quantity of OPC. In addition to the larger sieved ash (No. 300 sieve) containing a noticeable proportion of large-sized SCBA particles, another compelling reason for the hydration reaction's hindrance is the fact that SCBA used here consisted of larger unburnt carbon fibers (as evidenced by its higher LOI; Table 1) [20]. Chemically, the quantity of SCBA exceeded what was required to react with lime formed during the hydration process of OPC, resulting in excess silica leaching out and compromising the compressive strength [73]. The decrease in the compressive strength is also attributable to the porous structures of the bagasse ash particles, which is

also evident from the results of the water absorption and UPV tests in Sections 3.4 and 3.5, respectively. The internal matrix thus loses its capacity to withstand compressive loading [22,74,75]. The addition of 1.5% PP fibers to mix M2 improved the strength by 19% compared with mix M1 due to the densification activity of PP fibers and their lateral and radial reinforcements [53,76]. The densification of the internal matrix is witnessed from the results of the water absorption and UPV tests in Sections 3.4 and 3.5, respectively.

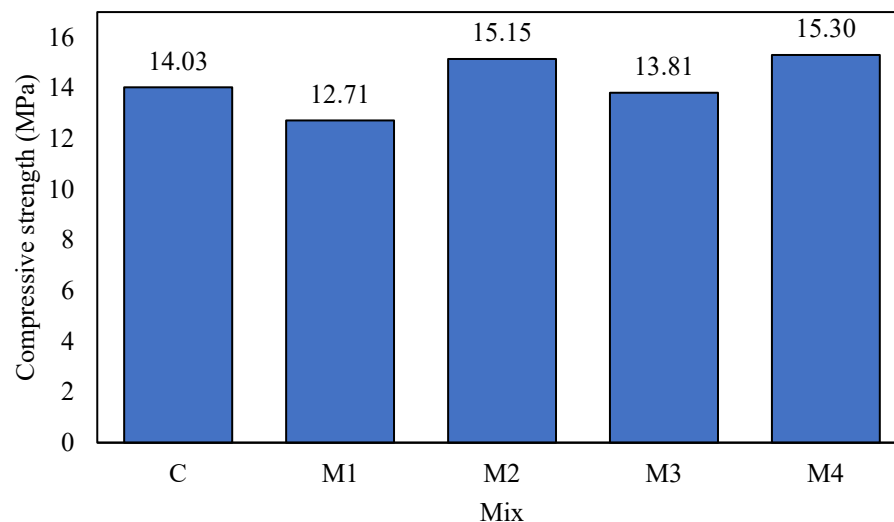


**Figure 6.** Compressive strength of developed composites after 28 days.

When compared with M2, the addition of CNTs (up to 0.04%) to M3 reduced the compressive strength. This could be related to the CNTs' hydrophilicity, in which they absorb water and impede the OPC hydration [77]. Moreover, because of the surface adherence of CNTs, CNTs could have attracted the SCBA particles, hence creating porous zones in the cement–sand matrix, leading to a decline in the compressive strength. As the concentration of CNTs was further increased to 0.08% in mix M4, the compressive strength was enhanced to 15.3 MPa. This is because CNTs functioned as nucleating agents during the OPC hydration, increasing the number of sites available for the hydration reaction and promoting the synthesis of hydration products including C-S-H [58]. This can, in turn, help fill the pores of the matrix overall.

Mortar cubes without fibers, when subjected to compressive loading, revealed a crushing failure, whereas when the fibers were added to the cubes, the failure mode changed from crushing to bulging failure, which may have been owing to lateral and radial reinforcements (confinement) by PP fibers, as depicted in Figure 7. Similar failure patterns for the specimens reinforced with PP fibers have been observed in the literature as well [78]. This behavior is also consistent with what reported by previous research for SCBA-based composites having PVA fibers [20].

The compressive strength of mortar is a crucial factor in determining the appropriate type of mortar for construction purposes. ASTM C270 [79] specifies the compressive strength for different types of mortars utilized in construction, such as the types M, S, N, and O. The determination of the appropriate type of mortar for a specific construction project is based on factors such as the required level of load-bearing capacity and the intended use of the structure [80]. For example, the type M mortar is specifically designed for applications where a high compressive strength is required. On the other hand, the type O mortar is suitable for low load-bearing structures where the compressive strength requirements are lower. Given the specifications set by ASTM C270 [79], it can be seen that all the mixes in this study exhibited the compressive strengths greater than the minimum threshold of 12.40 MPa for the type S mortar, and an even higher value of 15.30 MPa was achieved in the case of mix M4. Thus, it is inferred that the investigated mortars have a

variety of applications including masonry units, load-bearing walls, and other reinforced structural elements.



(a)

(b)

**Figure 7.** Failure modes under compressive loading: (a) Crushing (C and M1), (b) Bulging (M2–M4).

### 3.2. Flexural Strength Test

The flexural strength results are illustrated in Figure 8. The results of the flexural strength tests were consistent with those of the compressive strength tests, except the control mix that had the maximum strength. With the partial substitution of OPC with 15% SCBA, the flexural strength was decreased by 55%. This decrease is ascribed to the larger SCBA particles, which are porous and resulted in a weaker bond between the paste and aggregate interface [22,81]. In mix M2, the flexural strength was increased by 12%, which primarily was due to the densification and lateral and radial reinforcements provided by PP fibers, as elaborated earlier in Section 3.1.

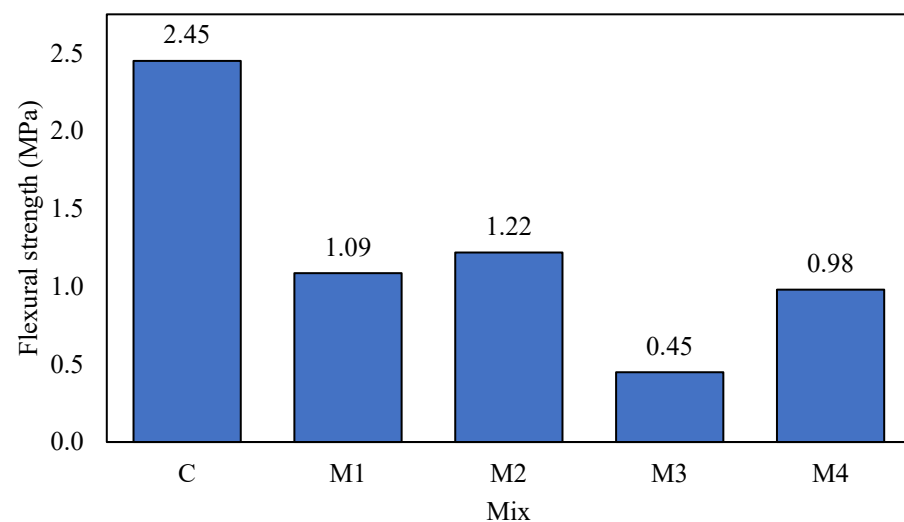


**Figure 8.** Flexural strength of developed composites after 28 days.

In mix M3, the flexural strength was decreased to 0.45 MPa with the initial incorporation of 0.04% CNTs, and in mix M4, the flexural strength was enhanced to 0.98 MPa when 0.08% CNTs were added. The reason for the changes in the flexural strength is similar to those of the compressive strength. CNTs initially hindered the hydration process due to their hydrophilic nature in mix M3 [77]. However, the flexural strength of both M3 and

M4 with CNTs was observed to be lesser compared with the mixes without CNTs. Further research is needed to understand the decreasing trend in the flexural strength as a result of adding CNTs.

The failure modes of the prisms are presented in Figure 9. C and M1 mixes (both without any fibers) exhibited brittle failures. The specimen broke down immediately after the peak load. In all the mixes, the concentration of the binder compared with sand was lesser. A lesser binder-to-sand ratio led to a weak bond between the cement–sand matrix and the fibers in mixes M2–M4 (which contained PP fibers), hence resulting in a fiber pullout failure. When the micro-cracks were developed at the bottom of the specimen due to the application of the load, PP fibers were ruptured owing to yielding, instead of bridging the cracks, leading to an immediate upward propagation of the cracks.



**Figure 9.** Failure modes of prisms under bending load: (a) Brittle failure in bending in C, (b) Fiber pullout failure in bending in M4.

### 3.3. Impact Strength Test

The impact strength results in the form of the modulus of toughness are indicated in Figure 10. The impact strength of the control mix (C) was the maximum, and when 15% SCBA was added as a partial replacement for OPC, the impact strength of mix M1 was decreased by 90%. Similar results have been given in the literature [22]. In mix M2, with the addition of 1.5% PP fibers by weight of the binder, the impact strength was improved to 0.073 MPa thanks to the energy absorption capacity of PP fibers [67].

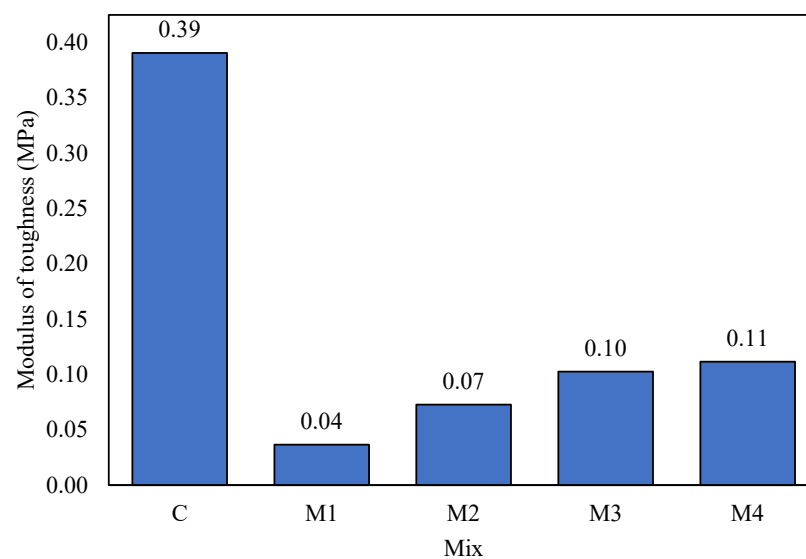


**Figure 10.** Impact strength in form of modulus of toughness of developed composites after 28 days.

Similarly, when 0.04% and 0.08% CNTs were added to mixes M3 and M4, respectively, the impact strength was enhanced further compared with M2 owing to the high impact resistance and toughness of CNTs [49]. This signified that the addition of CNTs to cementitious composites blended with SCBA and reinforced with PP fibers improved their resistance to an impact, shock, or blast loading, making them suitable for use in industrial floors, serving as foundations for vibrating machinery, runways for aircraft landings, bridges supporting vehicles, and explosion-proof structures.

### 3.4. Water Absorption Test

The results of the water absorption tests performed after 28 days are shown in Figure 11. The water absorption, when compared with the control mix, was increased by 4.7% with the replacement of 15% OPC with SCBA due to the porous zones created by SCBA in the cement–sand matrix [27,82]. Although in the literature, the volume of the voids both was increased and decreased with the inclusion of PP fibers followed by an increase and decrease in the permeability of the developed composites, respectively [76,83], the water absorption in the present research was decreased by 4.8% with the incorporation of PP fibers, which is an indication of a decrease in the volume of the voids.

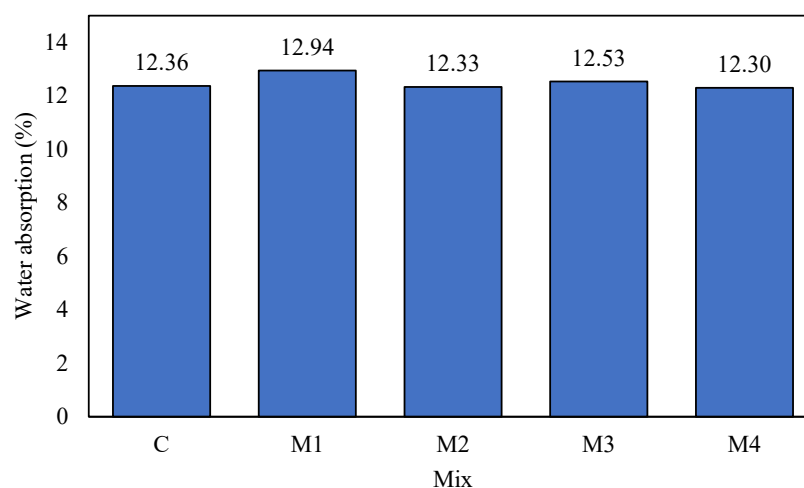


Figure 11. Water absorption of developed composites after 28 days.

When 0.04% CNTs by weight of the binder was added to mix M3, CNTs created a porous cement–sand matrix due to the interaction with SCBA, which caused the water absorption to increase to 12.53%. When 0.08% CNTs were added to mix M4, the water absorption was decreased to 12.3% owing to the densification of the internal matrix by CNTs filling the nanopores [47,51,65,78], which is also evident in the SEM micrographs as are to be described in detail in Section 3.6.

### 3.5. UPV Test

The results of the UPV tests, conducted to study the internal structure of the cementitious composites, are displayed in Figure 12. UPV of the control mix (C) was maximum but mix M1 demonstrated a decline of 44% due to the porous structure created by large-sized particles of SCBA in the internal matrix. Since the speed of sound is lesser in the air compared with in solids, UPV is reduced in cementitious composites with larger porosity [22,84,85]. UPV of mix M2 was increased by 1% compared with M1 with the addition of 1.5% PP fibers by weight of the binder, indicating the densification of the internal matrix owing to the inclusion of PP fibers [76,83]. The initial incorporation of 0.04% CNTs in mix M3 decreased UPV by 12% with respect to M2, while UPV of mix M4 was increased to 1555.21 m/s with an increase of 13% as compared with M3. The improvement in UPV of M4 with a higher content of CNTs was because of the pore densification action of CNTs. The SEM micrographs, as are to be described in Section 3.6, confirm this behavior. Both the

water absorption and UPV tests provided concrete evidence of the porous zones created by the additives, thus corroborating the results obtained from the mechanical tests.

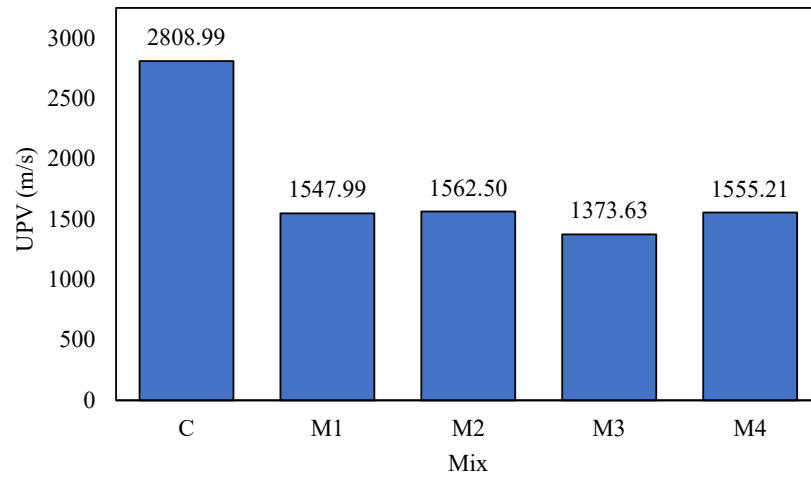
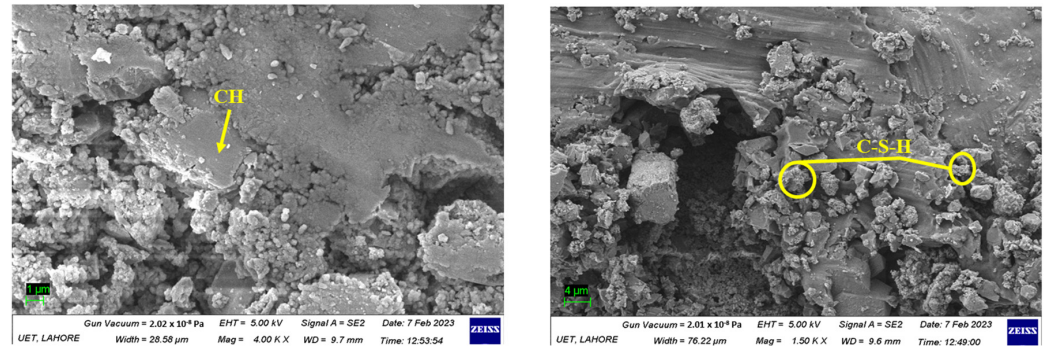


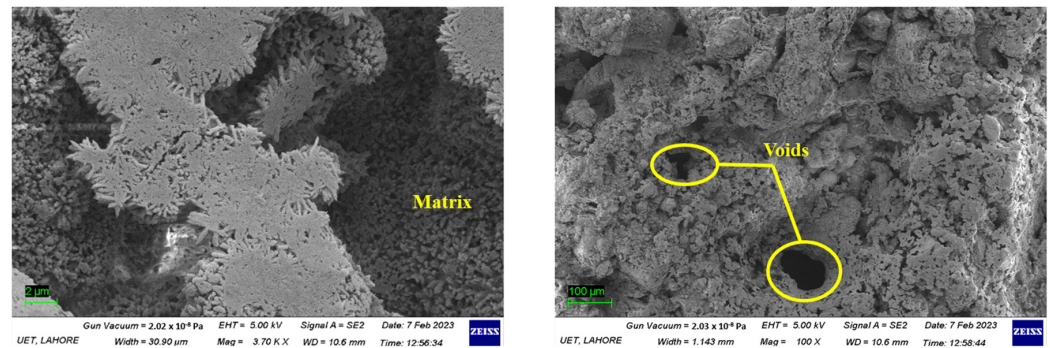
Figure 12. UPV results of developed composites after 28 days.

3.6. Microstructural Analysis

The SEM images of the developed cementitious composites at different magnifications, provided valuable insights into the composites’ microstructures and composition, are depicted in Figure 13.

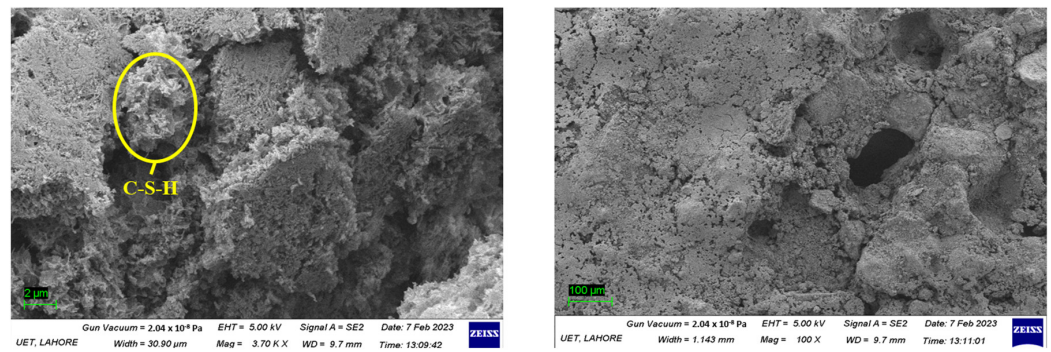


(a) C100-S0-P0-CN0 (C)

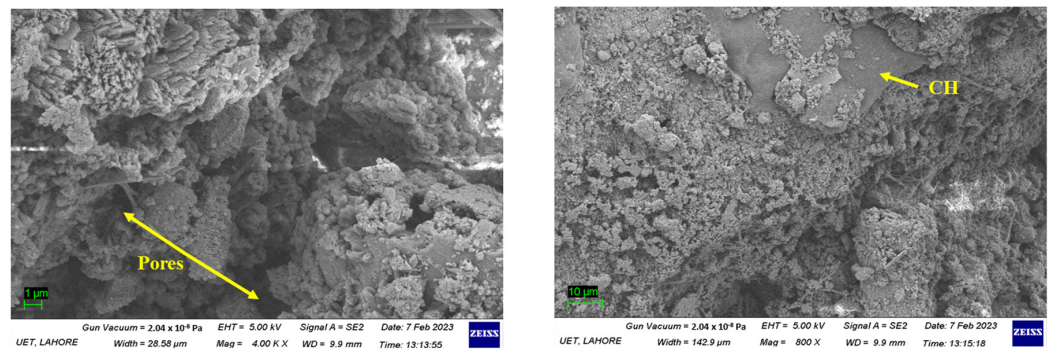


(b) C85-S15-P0-CN0 (M1)

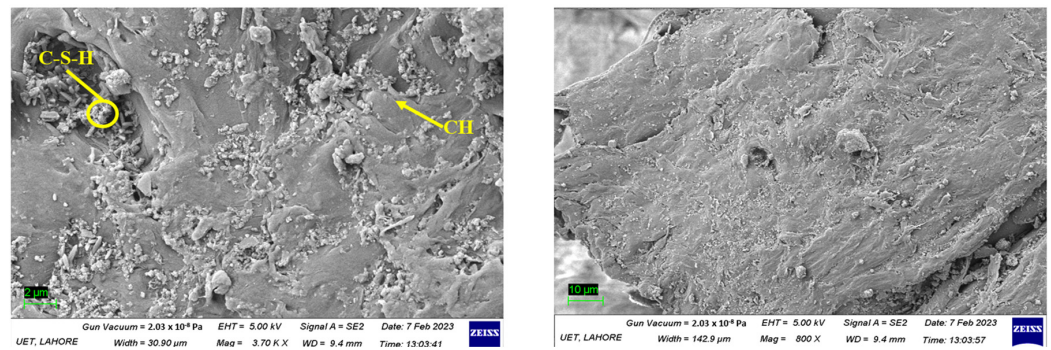
Figure 13. Cont.



(c) C85-S15-P1.5-CN0 (M2)



(d) C85-S15-P1.5-CN0.04 (M3)



(e) C85-S15-P1.5-CN0.08 (M4)

**Figure 13.** Results of SEM analysis.

The morphology and the elemental composition of the fractured samples illustrated the presence of hydration products mainly in the forms of C-S-H and C-H [7,86–91]. As shown in Figure 13a, C-S-H contributed to the formation of a denser and lower-porosity matrix [87,92]. C-H, as presented in Figure 13a,d,e, revealed the presence of a weak zone in the internal matrix [28,93]. On the other hand, the SEM analysis indicated the presence of the voids in the internal matrix, as displayed in Figure 13b, with the partial replacement of OPC with SCBA, which also increased the water absorption of the developed samples. The interaction between SCBA and CNTs could have created porous zones in the cement–sand matrix as a result of the surface adherence of CNTs (Figure 13d), which could explain why the compressive strength was lowered, as described earlier in Section 3.1.

The EDS results for the five developed mixes are demonstrated in Figure 14. For the current study, the elements of interest are carbon (C), silicon (Si), oxygen (O), and calcium (Ca).

Calcium, oxygen, and silicon signified the presence of CaO and SiO<sub>2</sub>, which revealed that C-H and C-S-H were formed during the hydration of OPC. The drops in the weights of calcium and silicon in M3, compared with mix M2, has made proof that MW-CNTs hindered the hydration process to some extent due to their hydrophilic nature, as depicted in Figure 14c,d. Moreover, Figure 14d,e showed a rise in the atomic weight of the carbon element in M3 and M4, indicating the existence of CNTs. As a result, the higher proportion of CNTs in the case of M4 could have filled in more pores in the matrix, leading to a more compact structure, as can be seen in Figure 14e, and thus, a higher compressive strength was achieved.

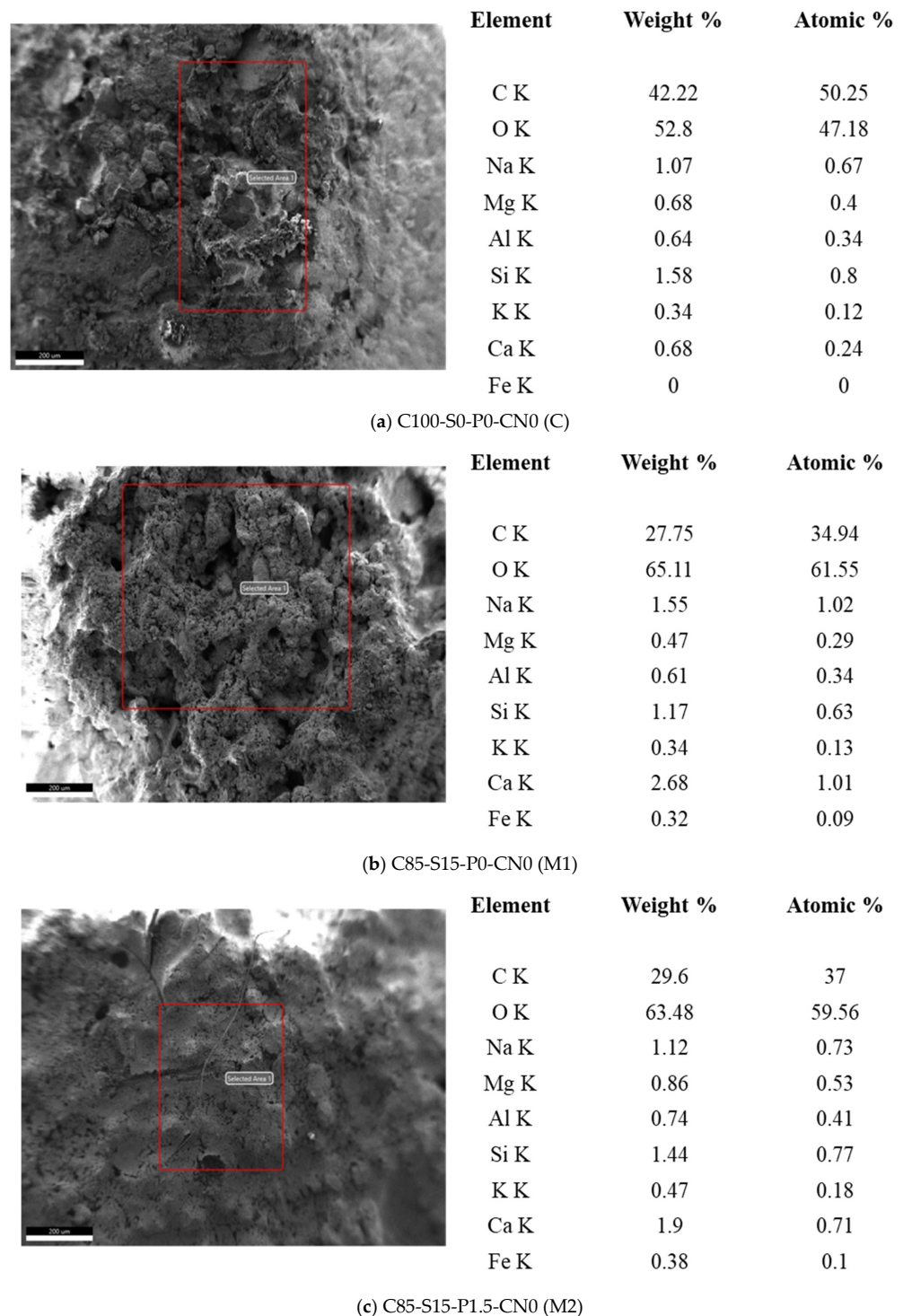
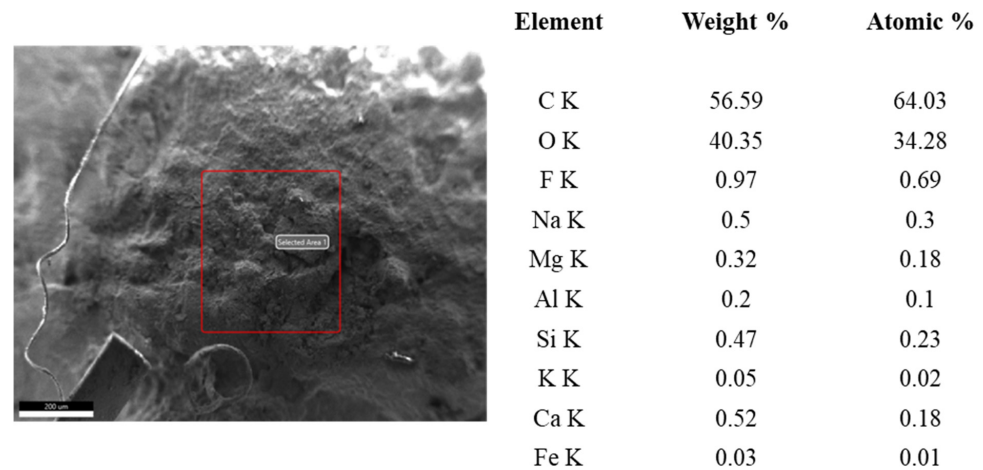
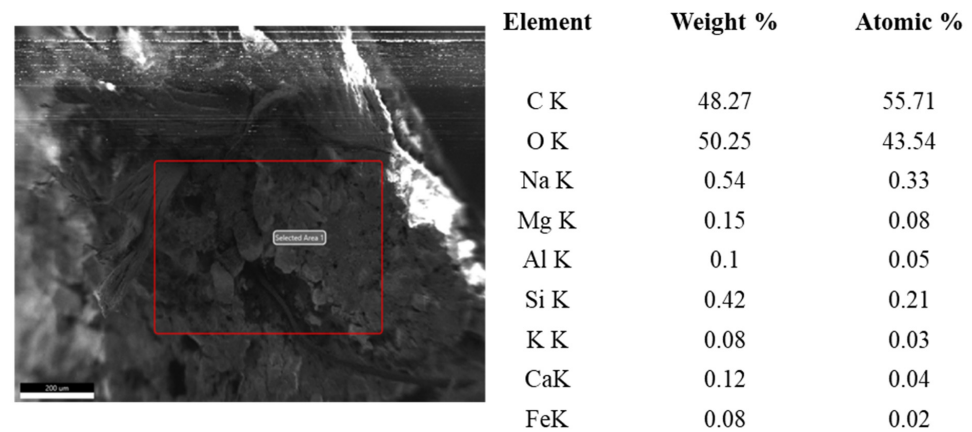


Figure 14. Cont.



(d) C85-S15-P1.5-CN0.04 (M3)



(e) C85-S15-P1.5-CN0.08 (M4)

**Figure 14.** EDS results of casted specimens.

#### 4. Conclusions

The current research focused on investigating the impact of varying CNTs, on SCBA-blended PP-fiber-reinforced cementitious composites. Based on the findings of this research work, the major conclusions are as follows:

- The partial replacement of OPC with SCBA led to decline in the compressive and flexural strengths, which were effectively compensated by PP fibers. Initially, the inclusion of 0.04% MW-CNTs posed challenges owing to their hydrophilic nature, resulting in a compromised hydration process and subsequent reduction in the strength. However, in the mix with 0.08% CNTs, higher compressive and flexural strengths of 15.30 MPa and 0.98 MPa were obtained, respectively, which can be used in general construction works such as masonry units, load-bearing walls, and other reinforced structural elements. This revealed that the incorporation of 15% SCBA, 1.5% PP fiber, and 0.08% CNTs by weight of the binder in the development of cementitious composites can play a substantial role in enhancing the sustainability and economy of the construction sector.
- The impact strength was decreased due to the poor energy absorption capabilities of SCBA. However, CNTs and PP fibers, with their toughness and energy absorption capabilities, improved the impact resistance of the specimens.
- The water absorption and UPV served as indicators of the porosity in the developed specimens. The inclusion of SCBA produced a porous structure, whereas PP fibers densified the cementitious matrix. CNTs initially increased the porosity and then filled the nanopores as their concentration was increased.

- From SEM and EDS, it was observed that, owing to their hydrophilic nature, MW-CNTs, can hinder the hydration activity of the binder; however, an optimum concentration of CNTs can result in the formation of a denser cement–sand matrix and high-stiffness C-S-H.

Although this study has examined the effects of SCBA along with the inclusion of PP fibers and CNTs on the performance of cementitious composites, further in-depth research is required to produce green and cost-effective construction materials incorporating SCBA, PP fibers, and CNTs through advanced analytical methods such as thermogravimetric and differential analysis, X-ray diffraction, and mercury intrusion porosimetry. In addition, the chloride and sulfate resistances of cementitious composites incorporating SCBA, PP fibers, and CNTs can be worth studying in the future.

**Author Contributions:** M.A.I.: Conceptualization, methodology, validation, formal analysis, investigation, writing—original draft preparation, and writing—review and editing. U.U.S.: Conceptualization, validation, formal analysis, investigation, writing—review and editing, supervision, and project administration. A.B.: Conceptualization, methodology, validation, formal analysis, investigation, resources, writing—original draft preparation, writing—review and editing, supervision, and project administration. N.Y.: validation, investigation, writing—original draft preparation, and writing—review and editing. I.S.: validation and investigation. All authors have read and agreed to the published version of the manuscript.

**Funding:** This research received no external funding.

**Data Availability Statement:** Data will be made available on request.

**Conflicts of Interest:** The authors declare no conflict of interest.

## References

1. Andrew, R.M. Global CO<sub>2</sub> emissions from cement production, 1928–2018. *Earth Syst. Sci. Data* **2019**, *11*, 1675–1710. [[CrossRef](#)]
2. Heede, R. Tracing anthropogenic carbon dioxide and methane emissions to fossil fuel and cement producers, 1854–2010. *Clim. Chang.* **2014**, *122*, 229–241. [[CrossRef](#)]
3. Malhotra, V.M. Making Concrete “Greener” with Fly Ash. *Concr. Int.* **1999**, *21*, 61–66.
4. Nie, S.; Zhou, J.; Yang, F.; Lan, M.; Li, J.; Zhang, Z.; Chen, Z.; Xu, M.; Li, H.; Sanjayan, J.G. Analysis of theoretical carbon dioxide emissions from cement production: Methodology and application. *J. Clean. Prod.* **2022**, *334*, 130270. [[CrossRef](#)]
5. Malhotra, V.M. Introduction: Sustainable Development and Concrete Technology. *Concr. Int.* **2002**, *24*, 22.
6. Pade, C.; Guimaraes, M. The CO<sub>2</sub> uptake of concrete in a 100 year perspective. *Cem. Concr. Res.* **2007**, *37*, 1348–1356. [[CrossRef](#)]
7. Mindess, S.; Young, F.; Darwin, D. *Concrete*, 2nd ed.; Prentice-Hall: Upper Saddle River, NJ, USA, 2003.
8. Gupta, S.; Chaudhary, S. State of the art review on supplementary cementitious materials in India—II: Characteristics of SCMs, effect on concrete and environmental impact. *J. Clean. Prod.* **2022**, *357*, 131945. [[CrossRef](#)]
9. Cherki El Idrissi, A.; Paris, M.; Rozière, E.; Deneele, D.; Darson, S.; Loukili, A. Alkali-activated grouts with incorporated fly ash: From NMR analysis to mechanical properties. *Mater. Today Commun.* **2018**, *14*, 225–232. [[CrossRef](#)]
10. Mousavinezhad, S.; Gonzales, G.J.; Toledo, W.K.; Garcia, J.M.; Newton, C.M.; Allena, S. A Comprehensive Study on Non-Proprietary Ultra-High-Performance Concrete Containing Supplementary Cementitious Materials. *Materials* **2023**, *16*, 2622. [[CrossRef](#)]
11. Nili, M.; Afroughsabet, V. The effects of silica fume and polypropylene fibers on the impact resistance and mechanical properties of concrete. *Constr. Build. Mater.* **2010**, *24*, 927–933. [[CrossRef](#)]
12. Prošek, Z.; Nežerka, V.; Hlůžek, R.; Trejbal, J.; Tesárek, P.; Karra’a, G. Role of lime, fly ash, and slag in cement pastes containing recycled concrete fines. *Constr. Build. Mater.* **2019**, *201*, 702–714. [[CrossRef](#)]
13. Ray, T.; Ranjan Mohanta, N.; Hitesh Kumar, M.; Saikrishna Macharyulu, I.; Samantaray, S. Study of effect of temperature on behavior of alkali activated slag concrete. *Mater. Today Proc.* **2021**, *43*, 1352–1357. [[CrossRef](#)]
14. Ashraf, M.; Iqbal, M.F.; Rauf, M.; Ashraf, M.U.; Ulhaq, A.; Muhammad, H.; Liu, Q. Developing a Sustainable Concrete Incorporating Bentonite Clay and Silica Fume: Mechanical and Durability Performance. *J. Clean. Prod.* **2022**, *337*, 130315. [[CrossRef](#)]
15. Amin, M.N.; Ahmad, A.; Shahzada, K.; Khan, K.; Jalal, F.E.; Qadir, M.G. Mechanical and microstructural performance of concrete containing high-volume of bagasse ash and silica fume. *Sci. Rep.* **2022**, *12*, 5719. [[CrossRef](#)] [[PubMed](#)]
16. Dinesh, A.; Rubina, I.; Asmin Varsha, N.; Dhevdharshini, M.; Ramesh, C. Evaluation of the readiness of clay bricks with partially replaced rice husk ash. *Mater. Today Proc.* **2023**. [[CrossRef](#)]
17. Jagadesh, P.; Ramachandramurthy, A.; Murugesan, R.; Sarayu, K. Micro-analytical studies on sugar cane bagasse ash. *Sadhana* **2015**, *40*, 1629–1638. [[CrossRef](#)]

18. Mehmood, A.; Irfan-ul-Hassan, M.; Yaseen, N. Role of industrial by-products and metakaolin in the development of sustainable geopolymer blends: Upscaling from laboratory-scale to pilot-scale. *J. Build. Eng.* **2022**, *62*, 105279. [[CrossRef](#)]
19. Su, Q.; Xu, J. Mechanical properties of concrete containing glass sand and rice husk ash. *Constr. Build. Mater.* **2023**, *393*, 132053. [[CrossRef](#)]
20. Yaseen, N.; Sahar, U.; Bahrami, A.; Mazhar Saleem, M.; Ayyan Iqbal, M.; Saddique, I. Synergistic impacts of fly ash and sugarcane bagasse ash on performance of polyvinyl alcohol fiber-reinforced engineered cementitious composites. *Results Mater.* **2023**, *20*, 100490. [[CrossRef](#)]
21. Yaseen, N.; Irfan-ul-Hassan, M.; Saeed, A.-R.; Rizwan, S.A.; Afzal, M. Sustainable Development and Performance Assessment of Clay-Based Geopolymer Bricks Incorporating Fly Ash and Sugarcane Bagasse Ash. *J. Mater. Civ. Eng.* **2022**, *34*, 04022036. [[CrossRef](#)]
22. Zareei, S.A.; Ameri, F.; Bahrami, N. Microstructure, Strength, and Durability of Eco-Friendly Concretes Containing Sugarcane Bagasse Ash. *Constr. Build. Mater.* **2018**, *184*, 258–268. [[CrossRef](#)]
23. Memon, S.A.; Javed, U.; Shah, M.I.; Hanif, A. Use of Processed Sugarcane Bagasse Ash in Concrete as Partial Replacement of Cement: Mechanical and Durability Properties. *Buildings* **2022**, *12*, 1769. [[CrossRef](#)]
24. Payá, J.; Monzó, J.; Borrachero, M.V.; Tashima, M.M.; Soriano, L. Bagasse Ash. In *Waste and Supplementary Cementitious Materials in Concrete*; Elsevier: Amsterdam, The Netherlands, 2018; pp. 559–598. [[CrossRef](#)]
25. Ribeiro, D.V.; Morelli, M.R. Effect of Calcination Temperature on the Pozzolanic Activity of Brazilian Sugar Cane Bagasse Ash (SCBA). *Mater. Res.* **2014**, *17*, 974–981. [[CrossRef](#)]
26. Torres Agredo, J.; Mejía de Gutiérrez, R.; Escandón Giraldo, C.E.; González Salcedo, L.O. Characterization of Sugar Cane Bagasse Ash as Supplementary Material for Portland Cement. *Ing. Investig.* **2014**, *34*, 5–10. [[CrossRef](#)]
27. Saad Agwa, I.; Zeyad, A.M.; Tayeh, B.A.; Adesina, A.; de Azevedo, A.R.G.; Amin, M.; Hadzima-Nyarko, M. A Comprehensive Review on the Use of Sugarcane Bagasse Ash as a Supplementary Cementitious Material to Produce Eco-Friendly Concretes. *Mater. Today Proc.* **2022**, *65*, 688–696. [[CrossRef](#)]
28. Bahurudeen, A.; Kanraj, D.; Gokul Dev, V.; Santhanam, M. Performance Evaluation of Sugarcane Bagasse Ash Blended Cement in Concrete. *Cem. Concr. Compos.* **2015**, *59*, 77–88. [[CrossRef](#)]
29. Khan, M.I.; Abdy Sayyed, M.A.; Ali, M.M.A. Examination of Cement Concrete Containing Micro Silica and Sugarcane Bagasse Ash Subjected to Sulphate and Chloride Attack. *Mater. Today Proc.* **2021**, *39*, 558–562. [[CrossRef](#)]
30. Thomas, B.S.; Yang, J.; Bahurudeen, A.; Abdalla, J.A.; Hawileh, R.A.; Hamada, H.M.; Nazar, S.; Jittin, V.; Ashish, D.K. Sugarcane Bagasse Ash as Supplementary Cementitious Material in Concrete—A Review. *Mater. Today Sustain.* **2021**, *15*, 100086. [[CrossRef](#)]
31. Akbar, A.; Farooq, F.; Shafique, M.; Aslam, F.; Alyousef, R.; Alabduljabbar, H. Sugarcane Bagasse Ash-Based Engineered Geopolymer Mortar Incorporating Propylene Fibers. *J. Build. Eng.* **2021**, *33*, 101492. [[CrossRef](#)]
32. Latifi, M.R.; Biricik, Ö.; Mardani Aghabaglou, A. Effect of the Addition of Polypropylene Fiber on Concrete Properties. *J. Adhes. Sci. Technol.* **2022**, *36*, 345–369. [[CrossRef](#)]
33. Berenguer, R.A.; Capraro, A.P.B.; Farias de Medeiros, M.H.; Carneiro, A.M.P.; de Oliveira, R.A. Sugar Cane Bagasse Ash as a Partial Substitute of Portland Cement: Effect on Mechanical Properties and Emission of Carbon Dioxide. *J. Environ. Chem. Eng.* **2020**, *8*, 103655. [[CrossRef](#)]
34. Irshidat, M.R.; Al-Nuaimi, N.; Rabie, M. Hybrid Effect of Carbon Nanotubes and Polypropylene Microfibers on Fire Resistance, Thermal Characteristics and Microstructure of Cementitious Composites. *Constr. Build. Mater.* **2021**, *266*, 121154. [[CrossRef](#)]
35. Kavya Sameera, V.; Keshav, L. Properties and Performance of Steel Fiber Reinforced Concrete Beam Structure—Review. *Mater. Today Proc.* **2022**, *66*, 916–919. [[CrossRef](#)]
36. Shen, L.; Yao, X.; Di Luzio, G.; Jiang, M.; Han, Y. Mix Optimization of Hybrid Steel and Polypropylene Fiber-Reinforced Concrete for Anti-Thermal Spalling. *J. Build. Eng.* **2023**, *63*, 105409. [[CrossRef](#)]
37. Liu, Y.; Wang, L.; Cao, K.; Sun, L. Review on the Durability of Polypropylene Fibre-Reinforced Concrete. *Adv. Civ. Eng.* **2021**, *2021*, 6652077. [[CrossRef](#)]
38. Sohaib, N.; Seemab, F.; Sana, G.; Mamoon, R. *Using Polypropylene Fibers in Concrete to Achieve Maximum Strength*; Institute of Research Engineers and Doctors, LLC: New York, NY, USA, 2018; pp. 37–42. [[CrossRef](#)]
39. Mazaheripour, H.; Ghanbarpour, S.; Mirmoradi, S.H.; Hosseinpour, I. The Effect of Polypropylene Fibers on the Properties of Fresh and Hardened Lightweight Self-Compacting Concrete. *Constr. Build. Mater.* **2011**, *25*, 351–358. [[CrossRef](#)]
40. Akarsh, P.K.; Shrinidhi, D.; Marathe, S.; Bhat, A.K. Graphene Oxide as Nano-Material in Developing Sustainable Concrete—A Brief Review. *Mater. Today Proc.* **2022**, *60*, 234–246. [[CrossRef](#)]
41. Carmichael, M.J.; Arulraj, G.P. Impact Resistance of Concrete with Nano Materials. *Mater. Today Proc.* **2021**, *37 Pt 2*, 677–684. [[CrossRef](#)]
42. Kotop, M.A.; El-Feky, M.S.; Alharbi, Y.R.; Abadel, A.A.; Binyahya, A.S. Engineering Properties of Geopolymer Concrete Incorporating Hybrid Nano-Materials. *Ain. Shams. Eng. J.* **2021**, *12*, 3641–3647. [[CrossRef](#)]
43. Liew, K.M.; Kai, M.F.; Zhang, L.W. Carbon Nanotube Reinforced Cementitious Composites: An Overview. *Compos. Part A Appl. Sci. Manuf.* **2016**, *91*, 301–323. [[CrossRef](#)]
44. Wu, H.; Wang, C.; Yang, D.; Ma, Z. Utilizing Nano-SiO<sub>2</sub> for Modifying the Microstructure, Strength and Transport Properties of Sustainable Cementitious Materials with Waste Concrete Powder. *J. Build. Eng.* **2023**, *63*, 105522. [[CrossRef](#)]

45. Khan, S.A.; Ghazi, S.M.U.; Amjad, H.; Imran, M.; Khushnood, R.A. Emerging Horizons in 3D Printed Cement-Based Materials with Nanomaterial Integration: A Review. *Constr. Build. Mater.* **2024**, *411*, 134815. [[CrossRef](#)]
46. Han, B.; Sun, S.; Ding, S.; Zhang, L.; Yu, X.; Ou, J. Review of Nanocarbon-Engineered Multifunctional Cementitious Composites. *Compos. Part A Appl. Sci. Manuf.* **2015**, *70*, 69–81. [[CrossRef](#)]
47. Konsta-Gdoutos, M.S.; Aza, C.A. Self Sensing Carbon Nanotube (CNT) and Nanofiber (CNF) Cementitious Composites for Real Time Damage Assessment in Smart Structures. *Cem. Concr. Compos.* **2014**, *53*, 162–169. [[CrossRef](#)]
48. Xie, X.L.; Mai, Y.W.; Zhou, X.P. Dispersion and Alignment of Carbon Nanotubes in Polymer Matrix: A Review. *Mater. Sci. Eng. R Rep.* **2005**, *49*, 89–112. [[CrossRef](#)]
49. Daghash, S.M.; Soliman, E.M.; Kandil, U.F.; Reda Taha, M.M. Improving Impact Resistance of Polymer Concrete Using CNTs. *Int. J. Concr. Struct. Mater.* **2016**, *10*, 539–553. [[CrossRef](#)]
50. Xu, S.; Liu, J.; Li, Q. Mechanical Properties and Microstructure of Multi-Walled Carbon Nanotube-Reinforced Cement Paste. *Constr. Build. Mater.* **2015**, *76*, 16–23. [[CrossRef](#)]
51. Konsta-Gdoutos, M.S.; Metaxa, Z.S.; Shah, S.P. Highly Dispersed Carbon Nanotube Reinforced Cement Based Materials. *Cem. Concr. Res.* **2010**, *40*, 1052–1059. [[CrossRef](#)]
52. Mohsen, M.O.; Taha, R.; Abu Taqa, A.; Shaat, A. Optimum Carbon Nanotubes' Content for Improving Flexural and Compressive Strength of Cement Paste. *Constr. Build. Mater.* **2017**, *150*, 395–403. [[CrossRef](#)]
53. Nuaklong, P.; Boonchoo, N.; Jongvivatsakul, P.; Charinpanitkul, T.; Sukontasukkul, P. Hybrid Effect of Carbon Nanotubes and Polypropylene Fibers on Mechanical Properties and Fire Resistance of Cement Mortar. *Constr. Build. Mater.* **2021**, *275*, 122189. [[CrossRef](#)]
54. Andrade Neto, J.D.S.; Santos, T.A.; Pinto, S.d.A.; Dias, C.M.R.; Ribeiro, D.V. Effect of the Combined Use of Carbon Nanotubes (CNT) and Metakaolin on the Properties of Cementitious Matrices. *Constr. Build. Mater.* **2021**, *271*, 121903. [[CrossRef](#)]
55. Asil, M.B.; Ranjbar, M.M. Hybrid Effect of Carbon Nanotubes and Basalt Fibers on Mechanical, Durability, and Microstructure Properties of Lightweight Geopolymer Concretes. *Constr. Build. Mater.* **2022**, *357*, 129352. [[CrossRef](#)]
56. Han, G.; Xiang, J.; Jing, H.; Wei, X.; Gao, Y.; Chen, W. Carbon Nanotubes Assisted Fly Ash for Cement Reduction on the Premise of Ensuring the Stability of the Grouting Materials. *Constr. Build. Mater.* **2023**, *368*, 130476. [[CrossRef](#)]
57. Kordkheili, H.Y.; Hiziroglu, S.; Farsi, M. Physical and Mechanical Properties of Cement Composites Manufactured from Carbon Nanotubes and Bagasse Fiber. *Mater. Des.* **2012**, *33*, 395–398. [[CrossRef](#)]
58. Manzur, T.; Yazdani, N. Optimum Mix Ratio for Carbon Nanotubes in Cement Mortar. *KSCE J. Civ. Eng.* **2015**, *19*, 1405–1412. [[CrossRef](#)]
59. ASTM C128; Standard Test Method for Relative Density (Specific Gravity) and Absorption of Fine Aggregate. ASTM International: West Conshohocken, PA, USA, 2016. [[CrossRef](#)]
60. ASTM C33; Standard Specification for Concrete Aggregate. ASTM International: West Conshohocken, PA, USA, 2023. [[CrossRef](#)]
61. Chia, L.; Huang, Y.; Xia, W.; Lu, P.; Zhang, D. Carbon Nanotube (CNT) Reinforced Cementitious Composites Using Carboxymethyl Cellulose (CMC) Treatment for Enhanced Dispersion, Mechanical, and Piezoresistive Properties. *Constr. Build. Mater.* **2023**, *377*, 131104. [[CrossRef](#)]
62. Hu, Y.; Luo, D.; Li, P.; Li, Q.; Sun, G. Fracture Toughness Enhancement of Cement Paste with Multi-Walled Carbon Nanotubes. *Constr. Build. Mater.* **2014**, *70*, 332–338. [[CrossRef](#)]
63. Sáez de Ibarra, Y.; Gaitero, J.J.; Erkizia, E.; Campillo, I. Atomic Force Microscopy and Nanoindentation of Cement Pastes with Nanotube Dispersions. *Phys. Status Solidi (a)* **2006**, *203*, 1076–1081. [[CrossRef](#)]
64. Sobolkina, A.; Mechtcherine, V.; Khavrus, V.; Maier, D.; Mende, M.; Ritschel, M.; Leonhardt, A. Dispersion of Carbon Nanotubes and Its Influence on the Mechanical Properties of the Cement Matrix. *Cem. Concr. Compos.* **2012**, *34*, 1104–1113. [[CrossRef](#)]
65. Zhang, P.; Su, J.; Guo, J.; Hu, S. Influence of Carbon Nanotube on Properties of Concrete: A Review. *Constr. Build. Mater.* **2023**, *369*, 130388. [[CrossRef](#)]
66. De Almeida Carisio, P.; Dos Santos Mendonça, Y.G.; Soares, C.F.T.; Reales, O.A.M.; de Moraes Rego Fairbairn, E.; Filho, R.D.T. Dispersion of Carbon Nanotubes with Different Types of Superplasticizer as a Dispersing Agent for Self-Sensing Cementitious Materials. *Appl. Sci.* **2021**, *11*, 8452. [[CrossRef](#)]
67. Karimipour, A.; Ghalehnovi, M.; de Brito, J.; Attari, M. The Effect of Polypropylene Fibres on the Compressive Strength, Impact and Heat Resistance of Self-Compacting Concrete. *Structures* **2020**, *25*, 72–87. [[CrossRef](#)]
68. ASTM C109; Standard Test Method for Compressive Strength of Hydraulic Cement Mortars. ASTM International: West Conshohocken, PA, USA, 2017. [[CrossRef](#)]
69. ASTM C348-20; Standard Test Method for Flexural Strength of Hydraulic-Cement Mortars. ASTM International: West Conshohocken, PA, USA, 2021. [[CrossRef](#)]
70. ASTM E23; Standard Test Methods for Notched Bar Impact Testing of Metallic Materials. ASTM International: West Conshohocken, PA, USA, 2018. [[CrossRef](#)]
71. ASTM C1403-00; Standard Test Method for Rate of Water Absorption of Masonry Mortars. ASTM International: West Conshohocken, PA, USA, 2017. [[CrossRef](#)]
72. ASTM C597-16; Standard Test Method for Pulse Velocity Through Concrete. ASTM International: West Conshohocken, PA, USA, 2016. [[CrossRef](#)]

73. Srinivasan, R.; Sathiya, K. Experimental Study on Bagasse Ash in Concrete. *Int. J. Serv. Learn. Eng. Humanit. Eng. Soc. Entrep.* **2010**, *5*, 60–66. [[CrossRef](#)]
74. Chi, M. Effects of Sugar Cane Bagasse Ash as a Cement Replacement on Properties of Mortars. *Sci. Eng. Compos. Mater.* **2012**, *19*, 279–285. [[CrossRef](#)]
75. Jagadesh, P.; Ramachandramurthy, A.; Murugesan, R. Evaluation of Mechanical Properties of Sugar Cane Bagasse Ash Concrete. *Constr. Build. Mater.* **2018**, *176*, 608–617. [[CrossRef](#)]
76. Afroughsabet, V.; Ozbakkaloglu, T. Mechanical and durability properties of high-strength concrete containing steel and polypropylene fibers. *Constr. Build. Mater.* **2015**, *94*, 73–82. [[CrossRef](#)]
77. Musso, S.; Tulliani, J.-M.; Ferro, G.; Tagliaferro, A. Influence of Carbon Nanotubes Structure on the Mechanical Behavior of Cement Composites. *Compos. Sci. Technol.* **2009**, *69*, 1985–1990. [[CrossRef](#)]
78. Wang, J.; Li, Y.; Qiu, Z.; Zhang, Y. Experimental Research on Compressive Properties of Recycling Polypropylene (PP) Fiber Recycled Coarse Aggregate Concrete. *J. Build. Eng.* **2023**, *76*, 107403. [[CrossRef](#)]
79. ASTM C270; Standard Specification for Mortar for Unit Masonry. ASTM International: West Conshohocken, PA, USA, 2014. [[CrossRef](#)]
80. Razeman, N.A.; Itam, Z.; Beddu, S.; Izam, N.S.M.N.; Ramli, M.Z.; Syamsir, A.; Mohamad, D.; Kamal, N.L.M.; Usman, F.; Asyraf, M.R.M. A Review on The Compressive Strength and Workability of Concrete with Agricultural Waste Ash as Cement Replacement Material. *IOP Conf. Ser. Earth Environ. Sci.* **2023**, *1135*, 012058. [[CrossRef](#)]
81. Batool, F.; Masood, A.; Ali, M. Characterization of Sugarcane Bagasse Ash as Pozzolan and Influence on Concrete Properties. *Arab. J. Sci. Eng.* **2020**, *45*, 3891–3900. [[CrossRef](#)]
82. Rukzon, S.; Chindapasirt, P. Utilization of Bagasse Ash in High-Strength Concrete. *Mater. Des.* **2012**, *34*, 45–50. [[CrossRef](#)]
83. Karahan, O.; Atiş, C.D. The Durability Properties of Polypropylene Fiber Reinforced Fly Ash Concrete. *Mater. Des.* **2011**, *32*, 1044–1049. [[CrossRef](#)]
84. Ikpong, A.A. The Relationship between the Strength and Non-Destructive Parameters of Rice Husk Ash Concrete. *Cem. Concr. Res.* **1993**, *23*, 387–398. [[CrossRef](#)]
85. Parihar, H.S.; Shanker, R.; Singh, V. Effect of Variation of Steel Reinforcement on Ultrasonic Pulse Velocity Prediction in Concrete Beam. *Mater. Today Proc.* **2022**, *65*, 1486–1490. [[CrossRef](#)]
86. Kirchheim, A.P.; Fernández-Altable, V.; Monteiro, P.J.M.; Dal Molin, D.C.C.; Casanova, I. Analysis of Cubic and Orthorhombic C3A Hydration in Presence of Gypsum and Lime. *J. Mater. Sci.* **2009**, *44*, 2038–2045. [[CrossRef](#)]
87. Lu, B.; Drissi, S.; Liu, J.; Hu, X.; Song, B.; Shi, C. Effect of Temperature on CO<sub>2</sub> Curing, Compressive Strength and Microstructure of Cement Paste. *Cem. Concr. Res.* **2022**, *157*, 106827. [[CrossRef](#)]
88. Maljaee, H.; Paiva, H.; Madadi, R.; Tarelho, L.A.C.; Morais, M.; Ferreira, V.M. Effect of Cement Partial Substitution by Waste-Based Biochar in Mortars Properties. *Constr. Build. Mater.* **2021**, *301*, 124074. [[CrossRef](#)]
89. Méducin, F.; Bresson, B.; Lequeux, N.; Noirfontaine, M.D.; Zanni, H. Calcium Silicate Hydrates Investigated by Solid-state High Resolution 1H and 29Si Nuclear Magnetic Resonance. *Cem. Concr. Res.* **2007**, *37*, 631–638. [[CrossRef](#)]
90. Tang, H.; Wu, X.; Xian, H.; Zhu, J.; Wei, J.; Liu, H.; He, H. Heterogeneous Nucleation and Growth of CaCO<sub>3</sub> on Calcite (104) and Aragonite (110) Surfaces: Implications for the Formation of Abiogenic Carbonate Cements in the Ocean. *Minerals* **2020**, *10*, 294. [[CrossRef](#)]
91. Wang, T.; Yi, Z.; Song, J.; Zhao, C.; Guo, R.; Gao, X. An Industrial Demonstration Study on CO<sub>2</sub> Mineralization Curing for Concrete. *iScience* **2022**, *25*, 104261. [[CrossRef](#)]
92. Le, D.H.; Sheen, Y.N. Assessment of Properties of Mortars Modified with Sugarcane Bagasse Ash Processed by Heating at Different Temperatures as Cement Replacement. *Eur. J. Environ. Civ. Eng.* **2022**, *27*, 393–415. [[CrossRef](#)]
93. Kazmi, S.M.S.; Munir, M.J.; Patnaikuni, I.; Wu, Y.F. Pozzolanic Reaction of Sugarcane Bagasse Ash and Its Role in Controlling Alkali Silica Reaction. *Constr. Build. Mater.* **2017**, *148*, 231–240. [[CrossRef](#)]

**Disclaimer/Publisher’s Note:** The statements, opinions and data contained in all publications are solely those of the individual author(s) and contributor(s) and not of MDPI and/or the editor(s). MDPI and/or the editor(s) disclaim responsibility for any injury to people or property resulting from any ideas, methods, instructions or products referred to in the content.